DOI 10.1002/biot.200600123 Biotechnol. J. 2006, 1, 976–987

Research Article

Piezoelectric ink jet processing of materials for medical and biological applications

Jan Sumerel[1], John Lewis[2], Andy Doraiswamy[2], Leila F. Deravi[3], Sarah L. Sewell[3], Aren E. Gerdon[3], David W. Wright[3] and Roger J. Narayan[2]

[1]Dimatix Inc., Santa Clara, CA, USA
[2]Joint Department of Biomedical Engineering, University of North Carolina, Chapel Hill, NC, USA
[3]Department of Chemistry, Vanderbilt University, Nashville, TN, USA

Many advanced medical and biological devices require microscale patterning of cells, proteins, and other biological materials. This article describes the use of piezoelectric ink jet processing in the fabrication of biosensors, cell-based assays, and other microscale medical devices. A microelectromechanical system-based piezoelectric transducer was used to develop uniform fluid flow through nozzles and to prepare well-defined microscale patterns of proteins, monofunctional acrylate ester, sinapinic acid, deoxyribonucleic acid (DNA), and DNA scaffolds on relevant substrates. Our results demonstrate that piezoelectric ink jet deposition is a powerful non-contact, non-destructive additive process for developing biosensors, cell culture systems, and other devices for medical and biological applications.

Received 12 July 2006
Accepted 14 July 2006

Keywords: Biomaterials · Ink jet · Microarray · Piezoelectric · Tissue engineering

1 Introduction

Recent advances in tissue engineering, biological sensing, and biotechnology have resulted from two complementary forces. First, there is a natural evolution towards microscale patterning and rapid prototyping of materials as novel technologies become available. Second, patterned materials provide the capability for specific interactions with cells, proteins, DNA, viruses, and other biological structures. Micropatterned biological materials are not only essential in medicine and biology, they are also of increasing interest in microelectronics, microelectromechanical systems (MEMS), sensors, display units, and optoelectronic devices [1].

One possible application for microscale patterning of biomaterials is tissue engineering. The demand for replacement materials for damaged or diseased tissues has led to the development of this field, which involves creating tissue substitutes by placing living cells within three-dimensional hydrogels [poly(vinyl alcohol)], resorbable polymers [poly(lactic acid)], or naturally derived material scaffolds (collagen) that help guide development [2–5]. The cell-seeded structures are then placed in bioreactors that provide the nutrients that allow cells to multiply within the scaffold. The cellular structures in the three-dimensional scaffold are then implanted in the body, so that it can resume normal function. Rapid prototyping techniques are used to guide cell growth within scaffolds; for example, patterned growth factors or cytokines manipulate cell attachment and differentiation [6].

Patterning technologies may also benefit the fabrication of cell-based biosensors and biological assays. A biosensor is an analytical device that uses antibodies, enzymes, nucleic acids, microorganisms, isolated cells, or other biologically derived systems as a sensing element

Correspondence: Professor Roger J. Narayan, Joint Department of Biomedical Engineering, Campus Box 7575, University of North Carolina, Chapel Hill, NC 27599-7575, USA
E-mail: roger_narayan@unc.edu
Fax: +1-919-5133814

Abbreviations: **DAPI**, diaminidino-2-phenyl indole; **FT-IR**, Fourier transform infrared; **MAPLE DW**, matrix assisted pulsed laser evaporation direct write; **MEMS**, microelectromechanical system; **PZT**, lead zirconate titanate

[7, 8]. These devices may be used to monitor variations in chemical and biological environments. Cell-based assays have been considered for use in prescreening pharmacological agents, proteins, and nucleic acids. DNA, RNA, and protein arrays have been used in biosensors, immunoassays, cell-culture devices, drug delivery devices, and high throughput drug screening devices [9]. Rapid prototyping techniques like ink jet printing may allow for high-throughput production of patterned multiplexed biological materials without the use of masks, stamps, ribbons, or other costly and time-consuming conventional processing equipment.

Rapid prototyping is a materials processing technology originally developed approximately 30 years ago for the preparation of machine tool prototypes [10]. In rapid prototyping, three-dimensional structures are created by selectively joining materials in an additive manner. These technologies include layer-by-layer growth of solids, liquids, or powders. Rapid prototyping technologies are subcategorized into contact and non-contact deposition. Some commonly used rapid prototyping techniques in biomedical engineering include fused deposition modeling, stereolithography apparatus, selective laser sintering, laser direct writing, microcontact printing, and ink jet printing.

Solid-based rapid prototyping techniques involve the joining or fusing of extruded material [11, 12]. For example, in fused deposition modeling, material is melted and extruded into thin filaments on a mobile platform, which can operate along X-, Y-, and Z- planes. The filaments fuse together upon cooling [11]. One of the disadvantages of fused deposition modeling is high operating temperatures. As a result, patterning of many biological materials is precluded [7, 12]. In addition, materials prepared using this process exhibit very high porosities and poor mechanical properties. Several variants of the fused deposition modeling process have been developed to overcome these limitations, including precision extrusion manufacturing, low-temperature deposition manufacturing, and rapid prototyping robotic dispensing.

Liquid-based techniques involve selective solidification of material in the liquid phase [11]. For example, in stereolithography, a photocurable resin is selectively solidified upon exposure to UV laser radiation. In this technique, movement of a Z-height stage controls exposure of the laser to a liquid resin reservoir. The X- and Y-stage movements may be used to pattern the material in the Z-plane. The laser polymerizes the liquid resin layer to generate a layer of solidified material. The table is then lowered and another layer is selectively cured. This layer-by-layer buildup process is repeated until the desired three-dimensional structure is obtained. The structure is then removed from the liquid reservoir, baked, and cleaned. Several factors, including encoder resolution, table step height, laser spot size, and laser performance determine the resulting resolution of fabricated structures processed using this technique. In addition, the biological, chemical, and mechanical properties of the resins, breakdown products, diluents, and dispersants used in stereolithography may not be suitable for many medical and biological applications [13, 14].

Powder-based rapid prototyping techniques involve selective melting of powders or granules in a powder bed using a high-power laser. Prior to laser exposure, the powder is annealed to a temperature close to its transition melting point, such that only a small increase in temperature is required to cause localized melting. A three-dimensional object is formed by moving the height-adjustable table containing the powder bed after processing of each layer. This technique has been utilized to fabricate complex porous ceramic matrices suitable for implantation in a bone defect [15]. Many other materials, including nylon, polystyrene, and titanium, may also be processed using this technique. The technique has the capability to process 3-D structures with complex features, including overhangs and undercuts. However, materials processed using selective laser sintering generally exhibit high porosity and surface roughness, which may preclude its use in many medical applications.

Matrix-assisted pulsed-laser evaporation direct write (MAPLE DW), also known as laser forward transfer, has recently been used for sub-10-μm resolution patterning of cells, biological materials, and organic materials. The process is a variation of the MAPLE technique, which is used for thin film processing of polymeric biomaterials [16]. The MAPLE DW system utilizes an UV laser source, a ribbon, a receiving substrate, and an X-Y-Z translational stage. The biomaterial to be deposited is embedded in a UV-absorbing matrix material. The biomaterial-matrix mixture is then spin-coated onto an optically transparent quartz piece, which is known as the ribbon. A computer-guided laser selectively ablates the matrix, which propels less than 10 nL of the biomaterial from the ribbon to the substrate. This subtractive process operates at room temperature and ambient pressure. MAPLE DW is a flexible process that can be used to fabricate micropatterns at lower laser fluences or to provide annealing, cleaning, and micromachining at higher laser fluences.

The MAPLE DW process provides several advantages over other techniques, including: (i) enhanced cell-substrate adhesion, (ii) deposition under ambient conditions, (iii) the amount of material transferred can be quantitatively determined, and (iv) multilayered structures can be prepared by serial ablation of several ribbons. MAPLE DW has been used to create composite patterns of bioceramic and osteoblast-like cells, which have potential applications in orthopedic and dental tissue engineering [17]. Neuroblast-like B35 cells were deposited at several depths within protein gels; these structures may be used for regeneration of damaged peripheral nerves [18]. More recently, the MAPLE DW system has been used to machine microscale channels in agarose substrates. Chan-

nels with widths between 60 and 400 μm were filled with adhesive proteins and cells. The structures were delaminated from the agarose substrates, and free-standing cellular networks were obtained [19, 20].

Microcontact printing transfers a fluid film from a poly(dimethysiloxane) stamp onto a substrate [21]. Although the microcontact printing method may be used to create patterns at relatively low costs, it is plagued by stamp fatigue and resolution problems [22]. There is also evidence that the micropatterned surfaces produced using this technique continue to degrade after deposition [23]. This process may not be specific to the microcontact printing technique, and it may result from the use of materials to reduce adhesion between corresponding surface areas. Pattern resolution has been increased by employing a laser-scanning confocal microscope to pattern the photoresist used in the fabrication of the master stamp [24]. Moving this method to large scale use will require additional fabrication advances.

In contrast to other prototyping methods, ink jet printing is a relatively straightforward fabrication process. In general, many formats of 2-D drawings, pictures and structures can be converted to a bit map image. The resulting bit map image can then be rasterized into X- and Y-coordinates to deposit materials in a corresponding printed pattern. This high-resolution patterning technology has many potential biological and medical applications. For example, ink jet printing technology has recently been used to fabricate electronic, medical, optical, and polymeric devices [25, 26].

Ink jet printers can dispense fluid droplets with volumes in the picoliter to microliter range, and the volume is related to nozzle size. The resolution of patterns prepared using ink jet printing is determined by a number of factors, including ink viscosity, surface tension, droplet size and lateral resolution of the printer head [27]. The development of desktop thermal ink jet printers by Canon and Hewlett-Packard [28] drove ink jet technology from expensive industrial applications to universal availability. The chemical properties of inks determine their jettability in a printer. As a result, the inks are tailored specifically for the printing device that is employed. Surface tension and viscosity are two primary chemical properties that determine printing success. During droplet formation, energy is distributed between viscous flow, the drop surface tension, and the drop kinetic energy.

Syringe-solenoid ink jet printers contain a syringe pump and a microsolenoid valve. The syringe pump is used to compress the fluid in the reservoir. When opened, the solenoid valve creates a pressure wave that forces fluid through the orifice [29]. There are three types of solenoid dispensers: flow through, aspirate-dispense, and isolated. These printers cannot generate droplets in the picoliter range. As a result, they are primarily used for liquid dispensing on a large scale. These valves rapidly switch back and forth between their open and closed states in very small, rapid pulses to permit the flow of pressurized liquid. Microsolenoid valves demonstrate higher resolution patterns. Improving dispensing precision is obtained due to decrease in drop size after each valve closure. The capability for rapid actuation makes the solenoid type of dispenser ideal for non-stop reagent dispensing, These dispensers have become an integral component of high-throughput laboratory applications in pharmaceutical industries.

In thermal ink jet printers, the printhead includes a nozzle, heater, chamber (site of bubble growth), manifold, and restrictor (ink path from between manifold and chamber). The resistive element heats a plate to approximately 300°C. As a result, a bubble boils out from the fluid in the chamber. This process forces fluid out of the nozzle [30]. Ink flows from the restrictor to the chamber after the bubble shrinks. Thermal ink jet printers are subdivided into three groups based on the orientation between the plane of bubble formation and the ejection of the droplet: roof shooting (ejection and bubble formation are in same direction), back shooting (ejection and bubble formation are in opposite directions), and side shooting (ejection is perpendicular to bubble formation). Major fabrication advances have been made using thermal ink jet printing [26] due to the low cost and wide availability of printheads. However, the thermal ink jet process may cause damage to thermally sensitive materials used in biology and medicine.

In contrast, piezoelectric ink jet printers have demonstrated greater promise for use in rapid prototyping and patterning of materials for medical and biological applications. The pressing requirements for smaller drop sizes, faster printing speeds, lower device costs, higher precision of printed features, and higher resolution of printed features have led to the use of silicon MEMS techniques for fabrication of ink jet printheads. Silicon fabrication methods have provided both improved overall jet-to-jet uniformity and increased fluid resistance performance characteristics. The jet-to-jet uniformity increased drop placement accuracy. In addition, the expansion of the operating range provided higher ink throughput values. Since silicon is a chemically inert material, a broad range of jettable fluids, including graphic arts inks, functional inks, and biologically relevant materials may be processed using piezoelectric ink jet printing.

Piezoelectric ink jet printing is a thermally constant process that can be carried out at room temperature or in a localized cold environment. The piezoelectric printhead consist of a piezoelectric transducer, nozzles, manifolds, ink pumping chambers, and fluid inlet passages. When a voltage is applied to the lead zirconate titanate (PZT) piezoelectric transducer, the transducer deforms and creates mechanical vibrations. These vibrations create acoustic waves, which in turn force ink out of the chamber through the nozzle [31]. Piezoelectric print heads are categorized based on the deformation mode of the trans-

ducer (*e.g.*, squeeze mode, bend mode, push mode, or shear mode) [32]. For example, the ink jet cartridge in the Dimatix Materials Printer (Dimatix Inc., Santa Clara, CA, USA) is powered by a thin piezoelectric unimorph, which is constructed in the plane of the wafer. This structure consists of patterned PZT bonded to a silicon diaphragm [31]. Actuation of the PZT piezoelectric transducer is in the plane of the wafer (bender mode). A die consists of 16 individually addressable jets that release drops perpendicular to the wafer from an array of inline nozzles that are spaced 254 µm apart. The effective diameter of the nozzle is 21.5 µm, which provides a drop in the ~10 pL range.

The optimum viscosity for jettable fluids in piezo drop-on-demand printheads is ~8–14 mPas (8–14 cps). However, most biological materials exhibit very low viscosities (0.1–1 cps) and very high surface tension values (58–60 cps dynes/cm). As a result, it is important to be able to adjust the operating parameters of the ink jet printhead to successfully jet low viscosity fluids. For example, in the Dimatix Materials printing system, it is possible to adjust the frequency of the waveform, the voltage to individual nozzles, and the structure of the waveform that drives the movement of the PZT piezoelectric transducer. As discussed here, this piezeoelectric ink jet printing may be used to develop microscale patterns of materials for medical and biological applications. Streptavidin protein, monofunctional acrylate esters, sinapinic acid, DNA, and multiwalled carbon nanotube/DNA hybrid materials have been printed on technologically relevant substrates. The patterned materials have been examined using several characterization techniques, including optical microscopy, atomic force microscopy, electron microscopy, Fourier transform infrared (FT-IR) spectroscopy, PCR, and quartz crystal microbalance. Our results demonstrate that piezoelectric ink jet deposition is a powerful non-contact, non-destructive additive process for developing biosensors, cell culture systems, and other devices for medical and biological applications.

2 Ink Jet processing of streptavidin patterns

Rhodamine-conjugated streptavidin (Pierce Chemicals, Rockford, IL, USA) was dissolved in PBS (Fisher Scientific, Fair Lawn, NJ, USA) to create a 1.6 mM solution. Polysorbate 20 surfactant (1%; Fisher Scientific, Fair Lawn, NJ, USA) was added to isolate the water-soluble protein. Silicon, methyl cellulose, and borosilicate glass slides substrates were used in these studies. A piezoelectric ink jet materials printer (Dimatix) produced digitally fabricated microarrays. The protein solution was maintained at 28°C, purged through the printhead for uniform droplet formation and then calibrated at a constant velocity of 0.58 m/s for all nozzles prior to deposition. The time of flight (TOF) of the ~10-pL drops was recorded using a stroboscopic broad band white light emitting diode and a CCD camera with a high-resolution 4× magnification lens and a spectral response of greater than 60% between 400–700 nm. The camera's field of view is approximately 1.2 × 1.6 mm. The strobe frequency is matched to the waveform frequency, and the computer aided design/computer aided manufacturing (CAD/CAM) motion control software (Drop Manager, Dimatix) has a built-in variable delay and drop refresh rate controls. The protein solution was deposited at 13 V using an optimized waveform. The ink jetted protein patterns were stored at a temperature of 4°C prior to characterization. In addition, a drop-cast sample of the rhodamine-conjugated streptavidin protein was prepared for FT-IR spectroscopy studies (see below).

Ink jet patterns were initially imaged using a broadband emission white light emitting diode source and a CCD camera outfitted with a high-resolution 4× magnification lens, which is integrated into the materials deposition printer. FT-IR spectroscopy was performed using a 5000 series spectrometer (Mattson, Madison, WI, USA), which provides 4 cm^{-1} resolution. The absorption spectra (4000–500 cm^{-1}) was recorded for both the ink jet deposited protein and drop-cast streptavidin protein films as a control. Atomic force microscopy was performed using an N-scriptor system (Nanoink, Skokie, IL, USA). In this system, the scanning head provides a maximum scan range of 80 µm × 80 µm. The imaging was performed in contact mode using silicon nitride cantilevers (spring constant = 0.06 N m^{-1}) with integrated pyramidal tips. Linear and 3-D profiles were obtained using Nanorule data analysis (Nanoink). Optical fluorescent microscopy of the ink jetted protein patterns was performed using a DLMB upright microscope (Leica Microsystems, Wetzlar, Germany).

The appropriate jetting voltage, firing frequency, waveform, and viscosity for the streptavidin/PBS solution were determined after systematic studies using several deposition conditions. Figure 1a contains optical micrographs of streptavidin ink drops generated at 13 V, and Fig. 1b shows drop location measured from the nozzle plate at specific time points. The mass-velocity remained constant after an initial 25–30 µs period. An optical image of an ink jetted streptavidin array on a silicon substrate is shown in Fig. 2. Various grid spacings and 2-D patterns were obtained using Drop Manager. Figure 2a shows ~20-µm features prepared using ink jetting, and Fig. 2b shows ~60-µm features prepared using ink jetting. The spacing between the features was well controlled. Occasionally, feature overlap was observed. The dried 60-mm drops were imaged using contact mode atomic force microscopy. Figure 3a and b contain low and high resolution atomic force micrographs of the ink jetted streptavidin protein arrayed patterns, respectively. The ink jetted proteins exhibited randomly oriented peaks, troughs, and feature sizes. The streptavidin features varied in size from 3 to 8 µm. Figure 3b shows a clear contrast

Biotechnol. J. 2006, 1, 976–987

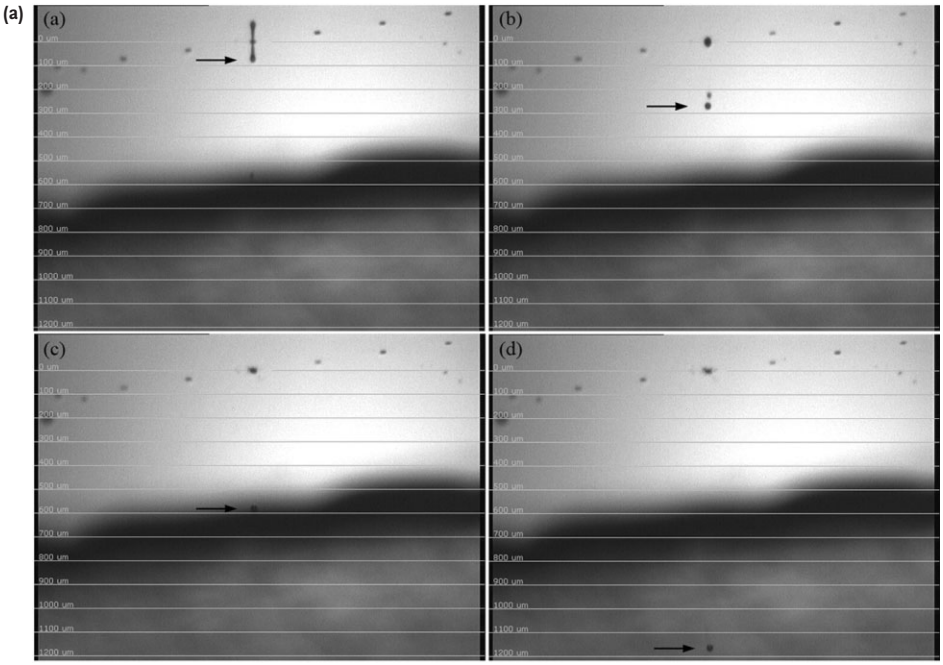

Figure 1. (a) Optical micrographs of streptavidin protein-ink jetting out of the nozzle plate. The droplets were captured at 20, 50, 100, and 200 µs. (b) Drop location measured from the nozzle plate at specific time intervals.

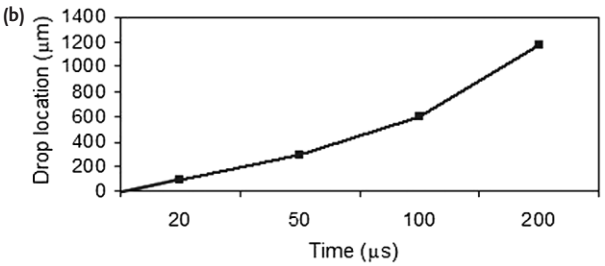

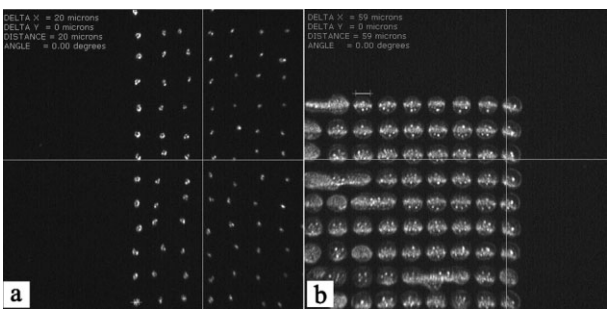

Figure 2. Optical micrographs of several ink jet-deposited streptavidin dot arrays, which contain different feature spacings.

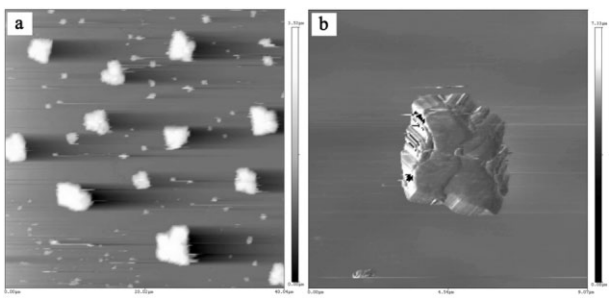

Figure 3. Contact mode atomic force micrographs of ink jet-deposited streptavidin arrays.

square-shaped streptavidin feature with a flat upper surface. Figure 4 contains a 3-D topography image of the protein patterns of Fig. 3a type pattern. A height profile of the protein structures shown in Fig. 5 indicates feature heights of approximately 2.2 µm with approximately 10-µm spacing. A high-resolution atomic force micrograph of the surface of the streptavidin feature in Fig. 3b is shown in Fig. 6. At a scan length of 0.67 µm on the feature surface, the Z-distance (peak to peak) was observed to be 0.68 µm with an average surface roughness of 0.092 µm. The atomic force micrographs demonstrated clear contrast images of the streptavidin patterns obtained by ink jetting. The distinctive micrometer-sized Z-heights and uniform smooth surfaces are unique to the piezoelectric ink jetting process. The streptavidin protein used in this study was labeled with rhodamine for imaging using fluorescence microscopy. Figure 7 shows fluorescence micrographs of a rhodamine-labeled streptavidin microarray prepared using ink jet printing. Feature sizes of approximately 20 µm were observed. Randomly oriented peaks, troughs, and feature sizes were observed in the patterned material. Figure 8a and b contain fluorescent micrographs at several resolutions of ink jetted streptavidin in a hatched-line pattern on a silicon substrate. The length of the line pattern was varied by altering the overlap of the droplets or the mass-velocity of the fluid. Developing this ink jet process further, we embedded proteins within a gel-like substrate. Figure 9a and b contain fluorescent micrographs of ink jetted streptavidin patterns at several resolutions. These figures suggest that streptavidin was embedded at variable depths within the methyl cellulose gel. To compare the native protein before and after jetting, FT-IR absorption spectra of ink jet de-

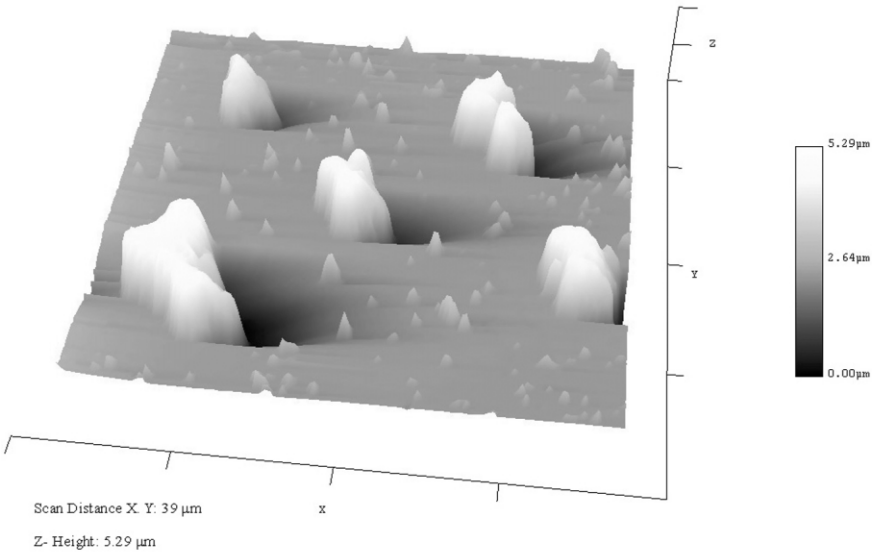

Figure 4. 3-D topographic image of the ink jet-deposited streptavidin microarrays (scan area 39 µm, Z-height 5.29 µm).

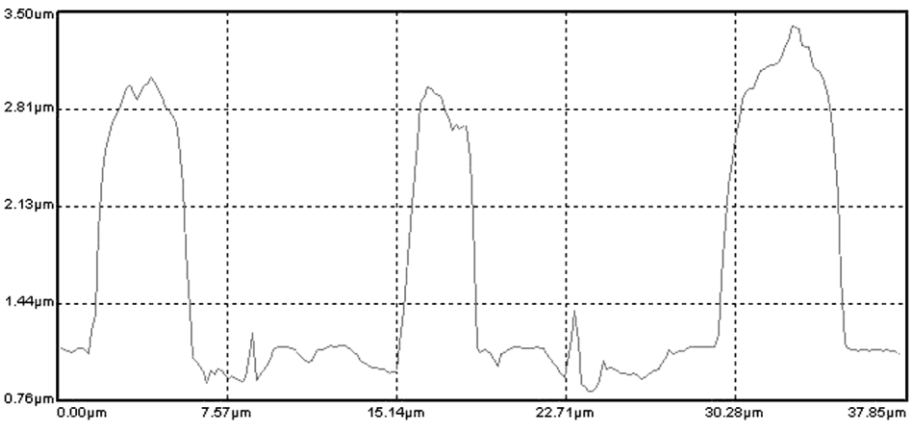

Figure 5. Height profile of streptavidin protein microarray, with features spaced approximately 10 µm apart.

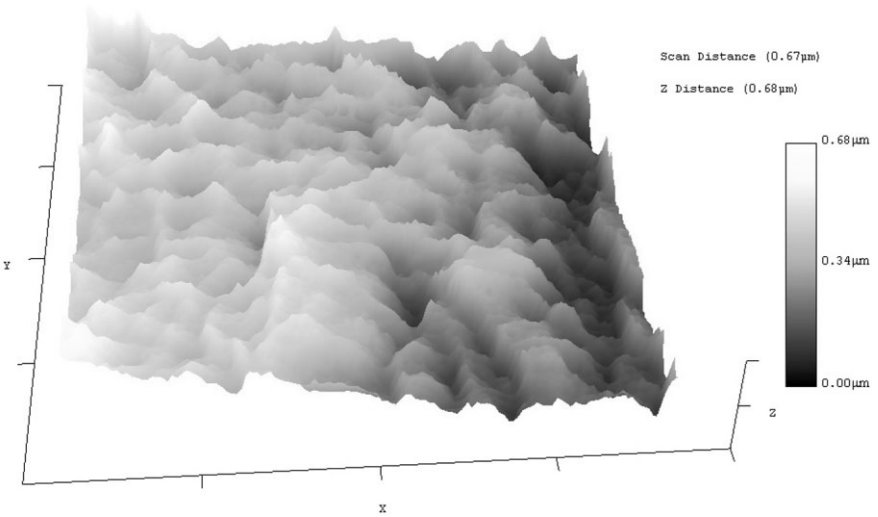

Figure 6. 3-D topographic image of ink jet-deposited streptavidin protein (scan size 0.67 µm, average surface roughness 0.09 µm).

posited and drop-cast streptavidin are shown in Fig. 10. Good correspondence between the peaks is observed. Slight differences in peak height were attributed to a variation in concentration between the drop-cast and ink jet-deposited samples. The observed peaks were identified and are listed in Table 1. Unlike many other high-throughput rapid prototyping techniques that require sample heating, piezoelectric ink jet deposition allows for rapid

Table 1. FT-IR absorption peaks for streptavidin protein deposited using piezoelectric ink jet printing

Notation	Peak wave number (cm^{-1})	Assignment
a	3476.0	Monosubstituted amide (O=C–NH)
b	2923.3	Strong amino acid zwitterions ($H3N^{+}$–CH–CO_2^{-})
c	2868.4	Secondary amine (CH_2–N)
d	1734.8	C=O stretching
e	1458.5	Aromatic ring stretching
f	1350.1	Weak amino acid zwitterions
g, h	1297.9, 1249.9	Aryl–NH
i	1110.8	CH_2–NH–CH_2
j	948.1	Conjugated thiol

deposition of heterogeneous microscale patterns of biomolecules. It is important to note that proteins were reproducibly printed using the MEMS device piezo ink jet printhead, and no obstruction of the printhead was observed.

3 Ink jet processing of monofunctional acrylate esters

Miniaturization of medical device packaging requires spatially controlled precise deposition of materials. UV/electron beam-cured coatings, inks, and adhesives are critical materials for these advanced devices [33]. The need for higher level packaging to increase board density and complexity also requires adhesive-specific technical advances [34]. Stenciling is one available technology for

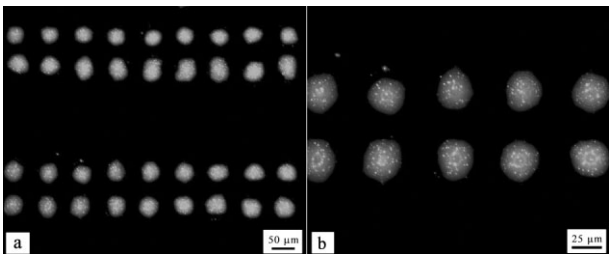

Figure 7. Optical fluorescent micrographs of rhodamine-labeled streptavidin deposited on a silicon substrate in a dot array pattern. Micrographs were obtained at several resolutions.

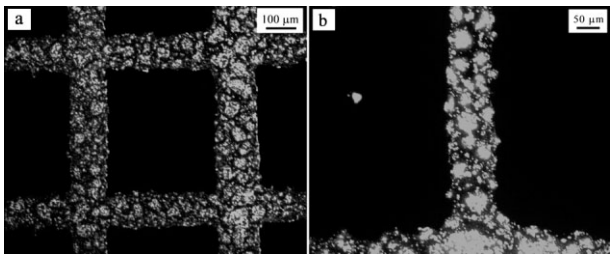

Figure 8. Optical fluorescent micrographs of rhodamine-labeled streptavidin protein deposited on a silicon substrate in a hatch pattern. Micrographs were obtained at several resolutions.

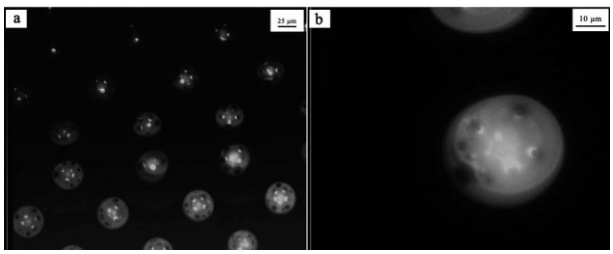

Figure 9. Optical fluorescent micrographs of rhodamine-labeled streptavidin protein deposited on a methyl cellulose gel in a dot array pattern. Micrographs were obtained at several resolutions.

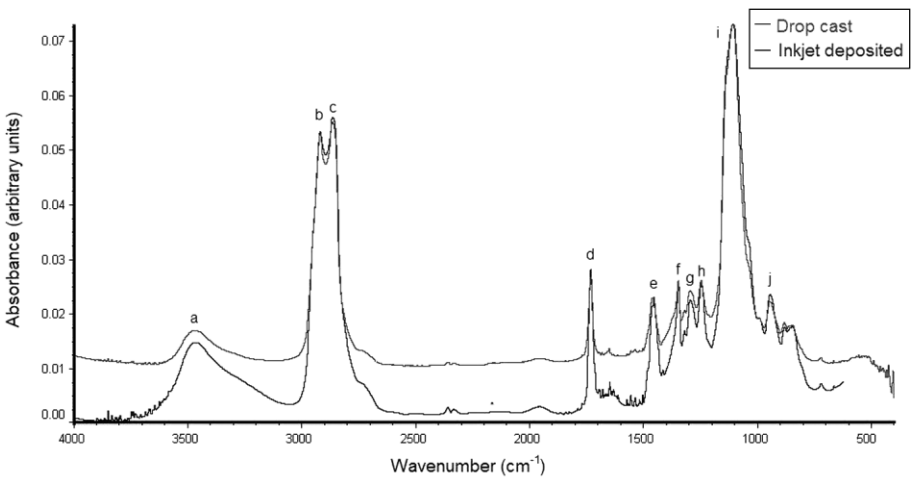

Figure 10. FT-IR absorption spectra overlay of ink jet-deposited and drop cast streptavidin protein.

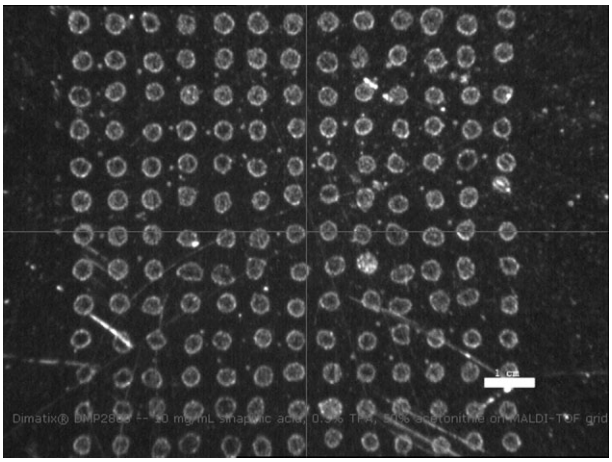

Figure 11. Optical micrograph of piezoelectric ink jet printed monofunctional acrylate ester on silicon wafer.

patterning of adhesives; however, there are disadvantages of this process, including (i) the typical dip and stamp set up involves the use of excessive amounts of adhesive, and (ii) there is no control of individual adhesive drop placement or volume. In addition, the stencils wear out over time, so deposition precision decreases with each stamping event. Ink jet printing of adhesives may allow for the precise deposition of these materials. We have deposited both thin films and arrays of Sartomer CD277 (Sartomer, Exton, PA, USA), a monofunctional acrylate ester. This material exhibit suitable chemical properties for piezoelectric ink jetting (surface tension = 28.5 dynes/cm, viscosity = 6 cps at 25°C), and was used in as-packaged form. Figure 11 shows an optical micrograph of the resulting drop pattern onto the silicon wafer. The resulting drops were approximately 56 µm each, and spacing between drops was approximately 266 µm. This ability to pattern an adhesive with drop sizes of <100 µm may advance the miniaturization of medical prostheses, electronics, and other advanced devices.

4 Ink jet processing of sinapinic acid

Methodologies for the analysis of tissues by MALDI-TOF MS have not been developed [35]. Dispensing accurate amounts of the matrix onto tissue using positional information will allow researchers to address specific subsections of the tissue. Analytes in MALDI are often incorporated into sinapinic acid matrices that absorb UV light and assist in removal of contaminants. Sinapinic acid (10 mg mL^{-1}) was dissolved in 0.3% TFA and 50% acetonitrile. The mixture was sonicated at room temperature for approximately 60 s, and then filtered through a 0.22-µm filter (Pall Life Sciences, Ann Arbor, MI). The fluid was then purged for 10 s. Next, 100% ethanol was drawn across the surface of the printhead before printing onto a gold-plated MALDI-TOF plate (Applied Biosystems, Foster City, CA). The fluid was printed into 340 drop patterns (spacing = 90 µm, width = 1.71 mm, height = 1.51 mm) (Fig. 12). These XY patterns were separated by 2.832 mm. The fluid was printed at a frequency of 1 KHz using a step-mode waveform. One nozzle operated at 20 V was used in these studies. Figure 13 contains the waveform used for printing of sinapinic acid patterns. A jetting pulse of 11.52 µs followed by a non-jetting pulse of 11.52 µs was used. The jetting pulse had a segment increase at a maximum of 3.58 µs, and this plateau ended at 7.29 µs. The waveform then decreased approximately 33% of total in approximately 1 µs, and linearly stabilized until 10.69 µs. The non-jetting waveform had a drop in pulse starting at 3.71 µs and ending at 10.69 µs. The jetting frequency maximum was 1 KHz, and the meniscus set point was at –3.0 inches H_2O. Calculated after drying, the average drop size was 44 µm. Future directions will be to use ink jetting to dispense picoliter volumes of sinapinic acid and couple it to MALDI-TOF MS.

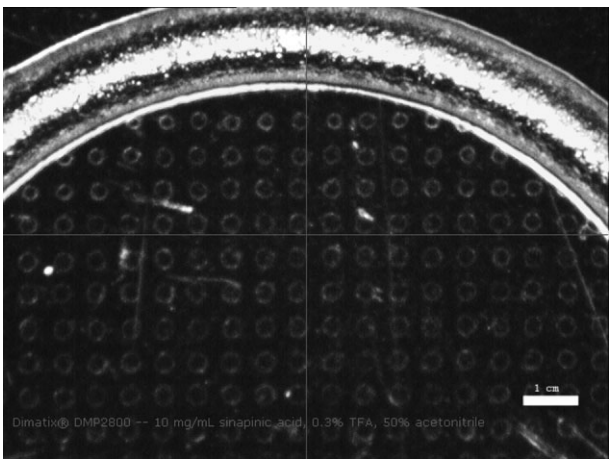

Figure 12. Optical micrograph of sinapinic acid printed on an MALDI-TOF plate.

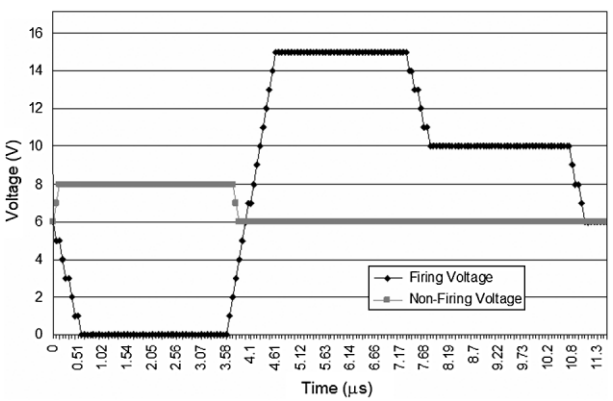

Figure 13. Piezoelectric ink jet waveform used during sinapinic acid ink jet printing.

5 Ink jet processing of DNA and amplification using PCR

Rapid detection employing microarray methods are necessary to biomedical and chemical sciences [36]. Miniaturization and automation of arrays may lead to decreased costs and faster analysis times [37]. As drop sizes decrease, feature sizes decrease and array densities increase. Many forensic samples obtained in the field have restricted amounts of recoverable material, and in some cases, two PCRs are required to reach the levels of sensitivity and verification required in the amplified DNA product [38]. Since piezoelectric ink jet printing only requires 10 pL per sample, the amount of DNA needed for a precise PCR assay is greatly reduced. For example, this technique may provide an important advance in studying the variation in a segment of mitochondrial DNA (a non-coding region between two transfer ribonucleic acid genes) [39]. Variations in this section of the gene is one obvious choice for forensic identification because of the large number of samples that are required [40], and the predominant isolated sample, human hair, shows low keratin protein variation between individuals [41]. Unlike contact printing techniques (*e.g.*, pin spotters) or expensive industrial ink jet printheads, the single-use ink jet printhead technology requires minimal deposition of fluids and minimal cross-contamination [37]. Human genomic DNA, 1.6 fg in 10 pL 50% ethanediol, was printed in the bottom of a 384-well assay plate and onto a silicon wafer in a 254-μm grid demonstrating drop placement accuracy (Fig. 14). Figure 15 demonstrates the high fidelity drop formation and the uniform drop speed when the DNA ink leaves the printhead nozzles. The samples were dried after printing. To test for PCR reliability, forward and reverse primers were printed onto the dried DNA. Next, a mixture containing 1× PCR buffer, 1.5 mm $MgCl_2$, 200 μM dNTPs, and Hot Start AmpliTaq Gold (Applied Biosystems) was printed for DNA amplification using standard PCR. PCR was done according to a standard protocol: 95°C for 5 min, followed by 30 cycles of 95°C for 30 s, 60°C for 30 s, and 72°C for 1 min. A 750-base pair fragment was resolved on a 1.2% agarose gel and visualized using ethidium bromide (Fig. 16). These successful results suggest that a significant cost savings may be obtained using piezoelectric ink jet printing of clinical microarrays. Miniaturization of the reaction, minimization of fluid volumes, and minimization of cross contamination may be obtained using this novel technology.

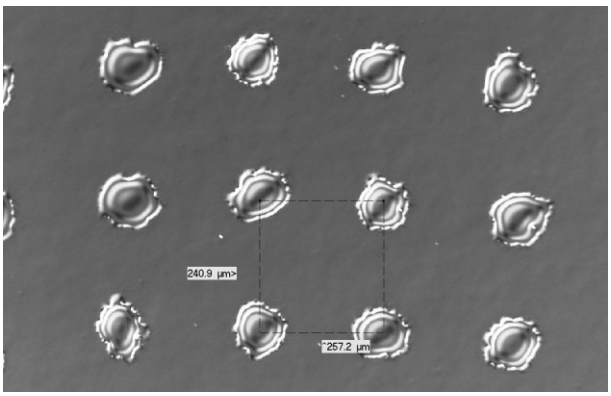

Figure 14. Optical micrograph of ink jet-deposited DNA pattern.

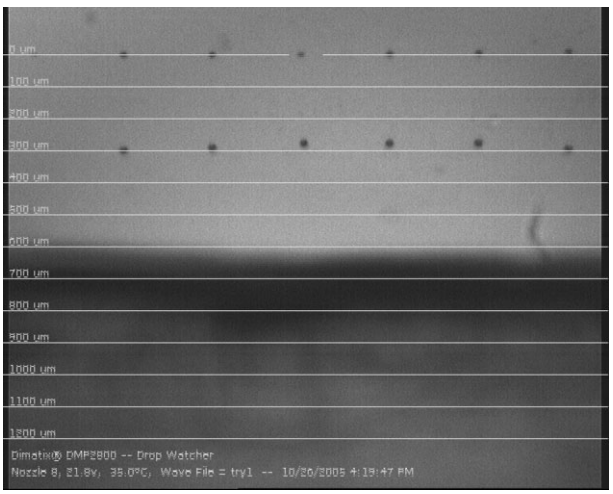

Figure 15. Optical micrograph of DNA ink jetting from the nozzle plate.

Figure 16. Ethidium bromide image of the DNA-agarose gel.

6 Ink jet processing of hybrid carbon nanotube/DNA composites

Hybrid composites are a class of materials with several novel applications [42]. These materials are employed in the fabrication of sensors [43], restorative dental materials [44], bone tissue engineering scaffolds, and heart valve tissue engineering scaffolds [45, 46]. One goal of ink jet printing is to generate thin films or 3-D structures of materials. Hybrid composites can be defined as inorganic nanoparticles mixed with organic polymers or organic polymers mixed with defined organic nanomaterials. A nucleic acid sensor has been generated by screen printing hybrid materials that contain multi-walled carbon nanotubes and nucleic acids [43]. Ye *et al.* [43] characterized a multi-walled carbon nanotube modified screen-printed carbon electrode using alternating current impedance. They demonstrated that this structure was able to detect direct electrochemical oxidation of adenine

residues of ribonucleic acid as well as well guanine or adenine residues of signal strand DNA. However, screen printing is inherently slow, wastes valuable materials, and is plagued by low resolution. In addition, once a screen is produced, it has to be stored until it is used again. In addition, if the pattern has changed, a new mask has to be produced for screen production. Marquette *et al*. [47] used screen printing to prepare an electrochemical biochip using a p53 target DNA sequence derived from exon 8 and graphite-containing ink. A detection limit of 1 nM (150 pg) was observed, suggesting inadequate sensitivity for *in vivo* p53 detection. Their results suggest that increased feature resolution is correlated with increased sensor sensitivity. Increased feature resolution may be obtained using ink jet printing. For example, piezoelectric ink jet printing with a 21-µm nozzle may provide an individual drop resolution of 40-µm resolution. On the other hand, screen printing typically provides ~100-µm resolution. While it has been shown that carbon nanotubes can be easily deposited using vapor deposition [48], the ability to pattern using this form is a subtractive process that does not lend itself to high throughput or flexibility. In contrast, piezoelectric ink jet printing of multi-walled carbon nanotubes is an additive process that is inherently flexible with respect to formation of patterns. High-resolution patterns of hybrid materials and other advanced sensor materials may be rapidly created using piezoelectric ink jet printing.

In this study, ink jet printing of hybrid composite containing multi-walled carbon nanotubes and DNA was demonstrated. Multiwalled carbon nanotubes (1 mg ml^{-1} , outer diameter 20–30 nm, wall thickness 1–2 nm, length 0.5–2 µm; Sigma Aldrich, St. Louis, MO, USA) were mixed in a 53% polypropylene glycol 400, 45% propylene carbonate solution containing 0.01% tetramethyl-5-decyne-4,6-diol, 2,4,7,9-propanol (Surfynol 104PA; Air Products, Allentown, PA, USA), 1 mg ml^{-1} salmon sperm DNA (Invitrogen, Carlsbad, CA, USA) and 1 µg ml^{-1} 4,6 diaminidino-2-phenyl indole (DAPI). The solution was sonicated in a water bath for 25 min at 37°C. After sonication, the mixture was filtered through a 0.22-µm syringe-tip filter (Pall Life Sciences, Ann Arbor, MI, USA). The solution was printed directly onto a gold sputter-coated 790-µm silicon wafer, a glass coverslip, or an aluminum scanning electron microscope puck using the same waveform that was shown in Fig. 13. During these studies, the voltage to the nozzle was maintained at 27 V. Average drop size onto a gold surface was 98.4 µm (SD = 5.4 µm). The multiwalled carbon nanotube/DNA hybrid patterns on a glass substrate were imaged using a Axiovert 200 inverted microscope (Carl Zeiss Inc., Thornwood, NY, USA) using a standard DAPI filter or dried at room temperature and examined by a S4200 scanning electron microscope (Hitachi, Tokyo, Japan). In Fig. 17, the bright field micrograph of a single drop of the hybrid composite (Fig. 17a) is compared to the DAPI staining (Fig. 17b). Figure 18a contains an

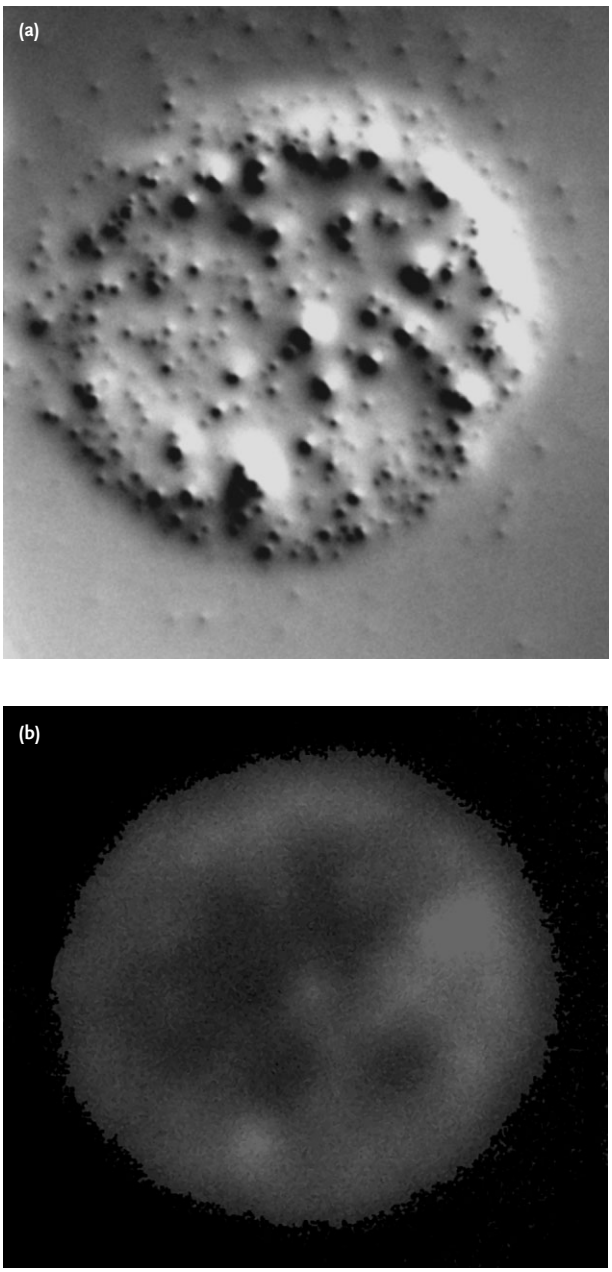

Figure 17. (a) Bright field image of a single drop of the hybrid multiwalled carbon nanotube /DNA pattern. (b) DAPI image of a single drop of the hybrid multiwalled carbon nanotube/DNA pattern.

electron micrograph of the sample printed using 254-µm spacing on a gold-sputtered silicon wafer. Figure 18a contains an electron micrograph of the sample printed using 126-µm spacing on an aluminum scanning electron microscopy puck. These images demonstrate that high resolution microscale features may be obtained using piezoelectric ink jet digital fabrication technology. Crystal quartz microbalance measurements of a 289-drop array were made using a research quartz crystal microbalance (Maxtek Inc., Beaverton, OR) and 9 MHz quartz crystals

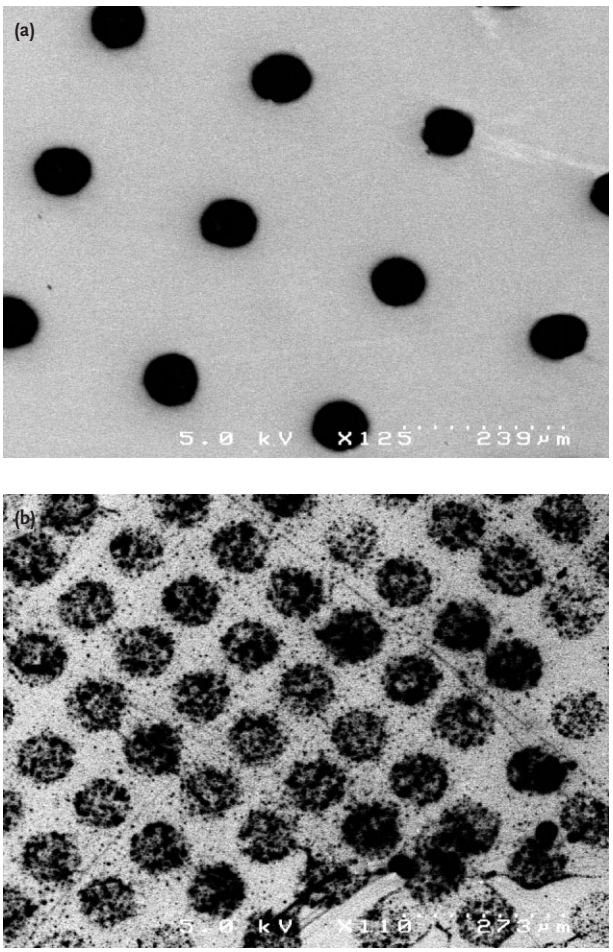

Figure 18. (a) Electron micrograph of ink jet-deposited hybrid multiwalled carbon nanotube/DNA pattern on gold-sputtered silicon wafer. (b) Electron micrograph of ink jet-deposited hybrid multiwalled carbon nanotube/DNA pattern on an aluminum substrate.

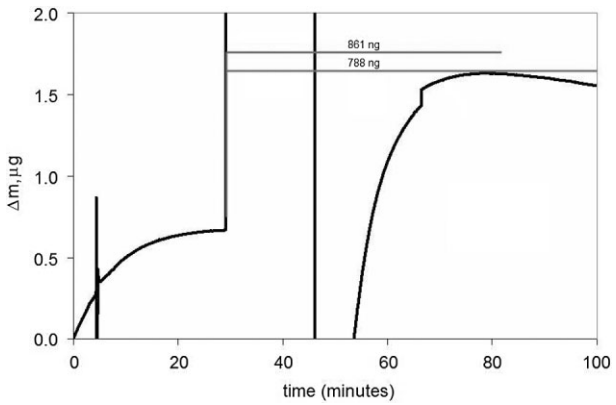

Figure 19. Weight measurements of hybrid multiwalled carbon nanotube/DNA using quartz crystal microbalance.

with chromium/gold electrodes. Baseline and adsorption frequency and resistance measurements were made after the electronics and the crystal were equilibrated. Resistance measurements were used to compensate for the density and viscosity effects of the contact solution. Frequency was converted to mass according to the Sauerbrey equation and previously known sensitivity factor (527 Hz/µg). It was shown that the 289-single-drop array provided a mass of 861 ng (a mass per drop of 2.978 ng) (Fig. 19). This printing process was greatly simplified by the ability of the Materials Printer to manipulate the waveform and voltage to an individual nozzle.

7 Conclusions

Piezoelectric ink jet printing is a powerful non-contact, non-destructive rapid prototyping technique for processing materials used in medicine and biology. In contrast to thermal ink jet printing, MEMS-constructed piezoelectric ink jet printheads use a patterned PZT piezoelectric transducer bonded to a silicon diaphragm to generate acoustic energy that drives drop formation. This novel, non-contact, and nondestructive printing process may be used to immobilize a variety of biological materials, while retaining their biological activity. We have demonstrated microscale patterning of several biological materials, including proteins, monofunctional acrylate ester, sinapinic acid, DNA, and DNA scaffolds. Streptavidin protein microarrays with well-defined microscale features were obtained, and the functionality of the patterned streptavidin was demonstrated. High-resolution patterns of sinapinic acid, a material used in MALDI-TOF MS, and monofunctional acrylate ester, a material used in miniaturized devices, were also prepared using piezoelectric ink jet printing. In addition, ink jet printing of hybrid composites may be used to immobilize nucleic acids, proteins, cells, and other biological materials in advanced medical devices. Piezoelectric ink jet printing is a unique rapid prototyping technique that offers great potential for developing biosensors, tissue substitutes, cell-culture systems, and several other advanced biomedical devices.

8 References

[1] Luesebrink, H., Glinsner, T., Jakeway, S. C. *et al.*, Transition of MEMS technology to nanofabrication. *J. Nanosci. Nanotechnol.* 2005, *5*, 864–868.

[2] Stock, U. A., Vacanti, J. P., Tissue engineering: current state and prospects. *Annu. Rev. Med.* 2001, *52*, 443–451.

[3] Vacanti, C. A., Vacanti, J. P., The science of tissue engineering. *Orthop. Clin. North Am.* 2000, *31*, 351–356.

[4] Cortesini, R., Stem cell, tissue engineering and organeogenesis in transplantation. *Transpl. Immunol.* 2005, *15*, 81–89.

[5] Yeong, W., Chua, C., Leong, K., Chandrasekaran, M., Rapid prototyping in tissue engineering: challenges and potential. *Trends Biotechnol.* 2004, *22*, 643–652.

[6] Sun, W., Pallavi, L., Recent development on computer aided tissue engineering – a review. *Comp. Methods Prog. Biomed.* 2002, *67*, 82–103.

[7] Hillberg, A. L., Brain, K. R., Allender, C. J., Molecular imprinted polymer sensors: implications for therapeutics. *Adv. Drug Deliv. Rev.* 2005, *57*, 1875–1889.
[8] Kane, R. S., Takayama, S., Ostuni, E., Ingber, D. E. *et al.*, Patterning proteins and cells using soft lithography. *Biomaterials* 1999, *20*, 2363–2376.
[9] Klefenz, H., Nanobiotechnology: from molecules to systems. *Eng. Life Sci.* 2004, *4*, 211–218.
[10] Kodama, H., Automatic method for fabricating a three-dimensional plastic model with photo-hardening polymer, *Rev. Sci. Instrum.* 1981, *52*, 1770–1773.
[11] Kai, C. C., Fai, L. F., Chu-Sing, L., *Rapid Prototyping: Principles and Applications,* 2nd edn., World Scientific Publishing, Singapore 2003.
[12] Hutmacher, D. W., Sittinger, M., Risbud, M. V., Scaffold-based tissue engineering: rationale for computer-aided design and solid free-form fabrication systems. *Trends Biotechnol.* 2004, *22*, 354–362.
[13] Despa, F., Orgill, D. P., Neuwalder, J., Lee, R. C., The relative thermal stability of tissue macromolecules and cellular structure in burn injury. *Burns* 2005, *31*, 568–577.
[14] Nishigori C., Cellular aspects of photocarcinogenesis. *Photochem. Photobiol. Sci.* 2006, *5*, 208–214.
[15] Vail, N. K., Materials for biomedical applications. *Mater. Design* 1999, *20*, 123–132.
[16] Pique, A., Wu, P., Ringeisen, B., Bubb, D. M. *et al.*, Processing of functional polymers and organic thin films by the matrix-assisted pulsed laser evaporation (MAPLE) technique. *Appl. Surf. Sci.* 2002, *186*, 408–415.
[17] Doraiswamy, A., Narayan, R. J., Harris, M. L., Qadri, S. B. *et al.*, Laser microfabrication of hydroxyapatite-osteoblast-like cell composites. *J. Biomed. Mater. Res. A* 2006, in press.
[18] Patz, T. M., Doraiswamy, A., Narayan, R. J., He, W., *et al.*, Three-dimensional direct writing of B35 neuronal cells. *J. Biomed. Mater. Res. B* 2006, *78*, 124–130.
[19] Doraiswamy, A., Patz, T. M., Narayan, R. J., Dinescu, M. *et al.*, Two-dimensional differential adherence of neuroblasts in laser micromachined CAD/CAM agarose channels. *Appl. Surf. Sci.* 2006, *252*, 4748–4753.
[20] Patz, T. M., Doraiswamy, A., Narayan, R. J., Modi, R., Chrisey, D. B., Two-dimensional differential adherence and alignment of C2C12 myoblasts. *Mat. Sci. Eng. B* 2005, *123*, 242–247.
[21] Jackman, R. J., Wilbur, J. L., Whitesides, G. M., Fabrication of submicrometer features on curved substrates by microcontact printing. *Science* 1995, *269*, 664–666.
[22] Xia Y., Rogers J. A., Paul K. E., Whitesides G. M., Unconventional methods for fabricating and patterning nanostructure. *Chem. Rev.* 1999, *99*, 1823–1848.
[23] Nelson, C. M., Raghavan, S., Tan, J. L., Chen, C. S., Degradation of micropatterned surfaces by cell dependent and independent process. *Langmuir* 2002, *19*, 1493–1499.
[24] Park, L. S., Seo, E. K, Young, R. D., Kim, K. *et al.*, Stamping lithography: printing without inks. *J. Am. Chem. Soc.* 2006, *128*, 858–865.
[25] Song, J. H., Nur, H. M., Defects and prevention in ceramic components fabricated by ink jet printing. *Mater. Proc. Technol.* 2004, *155–156*, 1286–1292.
[26] Lemmo, A. V., Rose, D. J., Tisone, T. C., Ink jet dispensing technology: applications in drug discovery. *Curr. Opin. Biotechnol.* 1998, *9*, 615–617.
[27] Xu, T., Gregory, C., Hickman, J. J., Boland, T. *et al.*, Ink jet printing of viable mammalian cells. *Biomaterials* 2005, *26*, 93–99.
[28] Calvert, P., Ink jet printing for materials and devices. *Chem. Mater.* 2001, *13*, 3299–3305.
[29] Haber C., Boillat M., van der Schoot B., Precise nanoliter fluid handling system with integrated high-speed flow sensor. *Assay Drug Dev. Technol.* 2005, *3*, 203–212.
[30] Bae, K. D., Baek, S. S., Lim, H. T., Kuk, K. *et al.*, Development of the new thermal head on SOI wafer. *Microelect. Eng.* 2005, *78–79*, 158–163.
[31] Menzel, C., NIP20: International Conference on Digital Printing Technologies, Salt Lake City Utah, 2005.
[32] Brünahl, J., Grishij, A. M., Piezoelectric shear mode drop-on-demand ink jet actuator. *Sensors Actuators A* 2002, *101*, 371–382.
[33] Myatt, C., Traggis, N., Dessau, K. L., Optical fabrication: optical contacting grows more robust. *Laser Focus World* 2006, *42*, 95–98.
[34] Ashmore, C., High-accuracy mass imaging for semiconductor die attach. *Adv. Packaging* 2006, *15*, 36.
[35] Umar, A., Dalebout, J. C., Timmermans, A. M., Foekens, J. A., Luider, T. M., Method optimisation for peptide profiling of microdissected breast carcinoma tissue by matrix-assisted laser desorption/ionisation-time of flight and matrix-assisted laser desorption/ionisation-time of flight/time of flight-mass spectrometry. *Proteomics* 2005, *5*, 2680–2688.
[36] Diehl, F., Beckmann, B., Kellner, N., Hauser, N. C. *et al.*, Manufacturing DNA microarrays from unpurified PCR products. *Nucleic Acids Res.* 2002, *30*, 79–84.
[37] Gutmann, O., Kuehlewein, R., Reinbold, S., Niekrawietz, R. *et al.*, A highly parallel nanoliter dispenser for microarray fabrication. *Biomed. Microdev.* 2004, *6*, 131–137.
[38] Vuorio, A. F., Sajantila, A., Hamalainen, T., Syvanen, A. C. *et al.*, Amplification of the hypervariable region close to the apolipoprotein B gene: application to forensic problems. *Biochem. Biophys. Res. Commun.* 1990, *170*, 616–620.
[39] Salas, A., Rasmussen, E. M., Laueu, M. V., Morling, N., Carracedo, A., Fluorescent SSCP of overlapping fragments (FSSCP-OF): a highly sensitive method for the screening of mitochondrial DNA variation. *Forensic Sci. Int.* 2001, *124*, 97–103.
[40] Wilson, M. R., Dizinno, J. A., Polanksey, D., Replogle, J., Budowle, B., Validation of mitochondrial DNA sequencing for forensic casework analysis. *Int. J. Legal. Med.* 1995, *108*, 68–74.
[41] Rodriguez-Calvo, M. S., Carracedo, A., Munoz, I., Concheiro, L., Isolectric focusing of human hair keratins: correlation with sodium dodecyl sulfate-polyacrylamide gel electrophoresis (SDS-PAGE): patterns and effect of cosmetic treatments. *J. Forensic Sci.* 1992, *37*, 425–431.
[42] Coe, S., Woo, W. K., Bawendi, M., Bulovi, V., Electroluminescence from single monolayers of nanocrystals in molecular organic devices. *Nature* 2002, *420*, 800–803.
[43] Ye, Y., Ju, H., Rapid detection of ssDNA and RNA using multiwalled carbon nanotubes modified screen-printed carbon electrode. Biosens. Bioelect. 2005, 21, 735–741.
[44] Anzai, M., Ishikawa, Y., Yoshihashi, K., Hirose, H., Nishiyama, M., Synthesis of organic-inorganic hybrid fillers at the molecular level and their application to composite resin. J. Oral Sci. 2002, *44*, 147–154.
[45] Stamm C., Khosravi A., Grabow N., Schmohl K. *et al.*, Biomatrix/polymer composite material for heart valve tissue engineering. Ann. Thorac. Surg. 2004, *78*, 2084–2092.
[46] Lee, S. J., Lim, G. J., Lee, J. W., Atala, A., Yoo, J. J., *In vitro* evaluation of a poly(lactide-co-glycolide)-collagen composite scaffold for bone regeneration. *Biomaterials* 2006, 27, 3466–3472.
[47] Marquette, C. A., Lawrence, M. F. and Blum, L. J., DNA covalent immobilization onto screen-printed electrode networks for direct label-free hybridization detection of p53 sequences. *Anal. Chem.* 2006, *78*, 959–964.
[48] Li, Y. L., Kinloch, I. A., Windle, A. H., Direct spinning of carbon nanotube fibers from chemical vapor deposition synthesis. *Science* 2004, *304*, 276–278.

